AIP Advances

Dramatic influence of Dy3+ doping on strain and domain structure in lead-free piezoelectric 0.935(Na1/2Bi1/2)TiO3−0.065BaTiO3 ceramics

C. Q. Li, Q. R. Yao, J. Z. Zhang, Z. G. Hu, F. F. Wang, A. Y. Liu, W. Z. Shi, and J. H. Chu

Citation: AIP Advances **5**, 127118 (2015); doi: 10.1063/1.4938514
View online: http://dx.doi.org/10.1063/1.4938514
View Table of Contents: http://scitation.aip.org/content/aip/journal/adva/5/12?ver=pdfcov
Published by the AIP Publishing

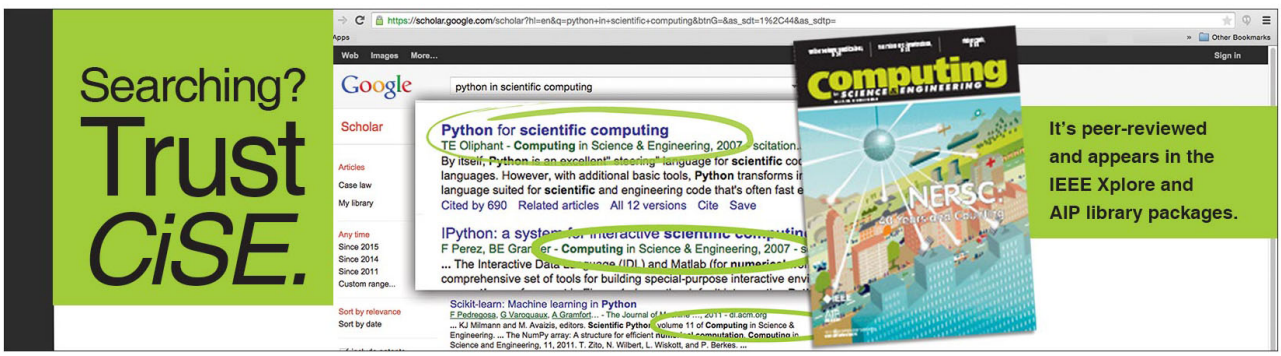

Dramatic influence of Dy^{3+} doping on strain and domain structure in lead-free piezoelectric $0.935(Na_{1/2}Bi_{1/2})TiO_3$–$0.065BaTiO_3$ ceramics

C. Q. Li (李传青),[1] Q. R. Yao (姚其容),[2] J. Z. Zhang (张金中),[1]
Z. G. Hu (胡志高),[1,a] F. F. Wang (王飞飞),[2] A. Y. Liu (刘爱云),[2]
W. Z. Shi (石旺舟),[2] and J. H. Chu (褚君浩)[1]
[1]*Department of Electronic Engineering, East China Normal University, Shanghai 200241, China*
[2]*Department of Physics, Shanghai Normal University, Shanghai 200234, China*

(Received 1 September 2015; accepted 7 December 2015; published online 17 December 2015)

An electric-field induced giant strain response and doping level dependent domain structural variations have been studied in the dysprosium (Dy^{3+})-modified $0.935(Na_{1/2}Bi_{1/2})TiO_3$-$0.065BaTiO_3$ (xDy:NBBT) ceramics with the doping levels of 0%, 0.5%, 1%, and 2%. X-ray diffraction and Raman spectroscopy analyses not only demonstrates the change in ionic configurations induced by Dy^{3+} doping, but also shows the local crystal symmetry for $x \geq 0.5\%$ doping levels to deviate from the idealized cubic structure. Piezoresponse force microscopy measurement exhibits the presence of an intermediate phase with orthorhombic symmetry at the critical Dy^{3+} doping level of 2%. Moreover, at this doping level, a giant recoverable nonlinear strain of ~0.44% can be observed with high normalized strain (S_{max}/E_{max}) of 728 pm/V. At the same applied field, the strain exhibits a 175% increase than that of NBBT ceramic. Such a large strain stems from the varying coherence lengths of polar nanoregions (PNRs) and an unusual reversible 90° domain switching caused by the symmetry conforming property of point defects, where the restoring force is provided by unswitchable defects. The mechanism reveals a new possibility to achieve large electric-field strain effect for a wide range of ferroelectric systems, which can lead to applications in novel "on-off" actuators. [http://dx.doi.org/10.1063/1.4938514]

Recently, enhanced piezoelectricity and large electric-field (E-field) induced strains have been successfully found in the $Na_{1/2}Bi_{1/2}TiO_3$ (NBT)-based ferroelectrics, which are considered the most promising environmental friendly alternatives to toxic Pb-based counterparts.[1–4] Around the morphotropic phase boundary (MPB), the $Na_{1/2}Bi_{1/2}TiO_3$-$BaTiO_3$ (NBBT), $Na_{1/2}Bi_{1/2}TiO_3$-$K_{1/2}Bi_{1/2}TiO_3$-$SrTiO_3$ (NBT-KBT-ST), as well as $Na_{1/2}Bi_{1/2}TiO_3$-$BaTiO_3$-$K_{1/2}Na_{1/2}NbO_3$ (NBT-BT-KNN) are nonpolar and cubic above the Curie temperature (T_c), yet become spontaneously polarized and mechanically distorted below T_c.[5–7] Indeed, typical ferroelectrics consist of complex domain patterns with different polarization directions, which can be switched under sufficiently large E-field. Accompanying the domain switching (90°/non-180° domains) is a huge strain due to the exchange of non-equal crystallographic axes.[8,9] Besides, these domain switching promotes the development of long-range ferroelectric order under the E-field. When E-field is applied along the $\langle 001 \rangle_c$ (c-cubic) crystallographic direction, the coherent length of the anti-phase ($a^-a^-a^-$) tilted regions increases and phase transition from cubic to tetragonal occurs. While along the $\langle 111 \rangle_c$ direction, the in-phase ($a^0a^0a^+$) oxygen octahedral tilted regions become broadening, which induce

[a]Author to whom correspondence should be addressed. Tel.: +86-21-54345150. Fax: +86-21-54345119. Electronic mail: zghu@ee.ecnu.edu.cn

the phase transition from cubic to rhombohedral phase.[10] Therefore, the evolution of the domains is proposed to explain the large strain and phase transitions in NBT-based ferroelectrics.

The basic approach to improve electrical properties of ferroelectrics is nonstoichiometry and doping with different elements. A modification of particular interest is dysprosium (Dy^{3+}) addition,[11,12] which tends to form $(Dy'_{Ti}\text{-}V_O^{\bullet\bullet})^{\bullet}$ defect dipoles with partially charge-compensating oxygen vacancies. When the doping level is close to the proximity of a concentration-induced phase transition between two ferroelectric phases, which causes the instability of the polarization state and the polarization direction can be easily rotated by external stress or *E*-field.[6] Various mechanisms such as "bulk effect", "domain wall effect" and "crystallite boundary effect" have been proposed to explain the configuration of defect dipoles and the interaction with domain walls.[13–15] However, the effects of defect dipoles caused by the introduction of Dy^{3+} on electrical properties and domain switching (90°/non-180° domains) in MPB composition of Dy^{3+}-modified $0.935(Na_{1/2}Bi_{1/2})TiO_3$-$0.065BaTiO_3$ (*x*Dy:NBBT) have not been well studied. In this letter, *E*-field induced large strain response, piezoelectricity and intricate domain structures of *x*Dy:NBBT ceramics have been investigated. Correspondingly, the mechanisms of the reversible domain switching and domain configuration during the phase transitions are discussed in detail.

The solid solutions *x*Dy:NBBT with Dy^{3+} doping levels of 0%, 0.5%, 1%, and 2% were synthesized by standard solid-state reaction sintering method. Stoichiometric mixture of analytical reagent grade powders Na_2CO_3(99.8%), $BaCO_3$(99.0%), Bi_2O_3(99.0%), TiO_2(98.0%), and Dy_2O_3(99.9%) were used as raw materials. The presintering was performed at 900 °C, and sintering was done at 1200 °C in air. The crystal structures were investigated by x-ray diffraction (XRD) using a Ni filtered Cu-Kα radiation operated at 40 kV and 200 mA (D/MAX-2550V, Rigaku Co.). The Raman scattering measurements were carried out by a Jobin-Yvon LabRAM HR 800 UV micro-Raman spectrometer. A laser with the wavelength of 632.8 nm was taken as the exciting source and the spectral resolution is better than 1 cm^{-1}. The laser beam was focused through a 50× microscope with a working distance of 18 mm. The ferroelectric hysteresis loops and bipolar strain curves were measured in silicon oil with the aid of a Sawyer-Tower circuit (TF2000 analyzer, Aixacct, Aachen, Germany). The domain structures were acquired using piezoresponse force microscopy (PFM, Cypher, Asylum Research).

Fig. 1(a) shows the XRD patterns of *x*Dy:NBBT (*x*=0-2%) specimens. All the ceramics exhibit a pure perovskite structure, which indicates that $BaTiO_3$ (BT) and Dy_2O_3 materials have diffused into the NBBT lattices. The diffraction patterns exhibit no profile shape asymmetry and no splitting sign, suggesting that these specimens belong to the rhombohedral phase. Recent *in situ* synchrotron study on NBBT indicated that unpoled NBT-0.065BT ceramic was ferroelectric rhombohedral at room temperature and significant rhombohedral to tetragonal distortion was only visible with the application of electric field above a certain threshold field level.[16,17] Close inspection of the diffraction peaks [Fig. 1(a) insets I and II], a shift of peaks towards to a higher diffraction angle is resulted from the fact that the ionic radius of Dy^{3+} (0.91 Å) is smaller than those of Bi^{3+} (1.17 Å) and Na^{+} (1.39 Å). However, one left shift anomaly can be collected for Dy^{3+} doping level of 2%. The phenomenon can be explained by TiO_6 octahedral tilting, which is caused by Dy^{3+} (0.91 Å) supersede Ti^{4+} (0.61 Å). It was reported that the Dy^{3+} ion occupying Ti^{4+} sites showed the typical acceptor-doped behavior up to the doping level of 2%,[18] which can be expressed by the following formula: $Bi_2O_3 + Dy_2O_3 \rightarrow 2Bi_{Bi} + 2Dy'_{Ti} + 6O_O + V_O^{\bullet\bullet}$. Also, the local distortions in the crystal structure can be extracted from various lattice constants. The value of lattice constant *a* decreases from 5.518 (Å) to 5.505 (Å) and then increases from 5.505 (Å) to 5.507 (Å) with increasing Dy^{3+} doping. However, the value of the rhombohedral lattice parameter *a* for 2%Dy:NBBT ceramic is still less than that of NBBT ceramic, which agree well with those by Zannen *et al*. reported.[12] Thus, one can expect that there will be different XRD patterns response for *x*Dy:NBBT ceramics with ferroelectric long-range order and short-range coherence phases, respectively.

Figs. 1(b)-1(e) show the Raman spectra of *x*Dy:NBBT and the corresponding Lorentzian-shaped deconvolution. Three main regions can be observed in the frequency range of 80-1000 cm^{-1}. The first one at around 260 cm^{-1} associates with A_1 mode (related to Ti-O bond vibrations). The relatively broadening phonon bands [e.g., $A_1^{(2)}$] and the overlapping of $A_1^{(1)}$ and $A_1^{(2)}$ Raman modes could be observed due to the B-site disorder caused by Dy^{3+} doping.[5] The mid-frequency region at

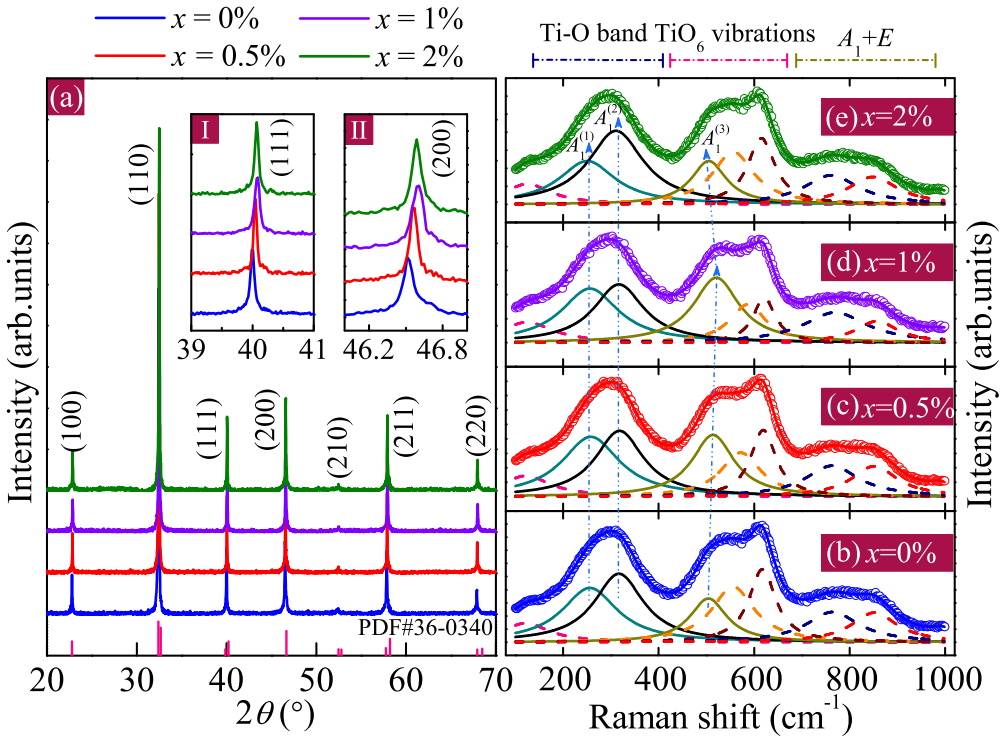

FIG. 1. (a) The XRD pattern of the *x*Dy:NBBT ceramics with different Dy^{3+} doping levels: $x = 0\%$, 0.5%, 1%, and 2%. The insets I and II represent the enlarged region for the diffraction peaks at $2\theta \approx 41°$ and 47°, respectively. (b)-(e) Room-temperature Raman spectra (dotted lines) and the corresponding Lorentzian fitting results (solid lines) for *x*Dy:NBBT (corrected by Bose-Einstein population factor) as a function of Dy^{3+} doping levels. The detailed assignment of the phonon modes is also plotted.

about 420~700 cm^{-1} is related to the vibration of the TiO_6 octahedra.[5,20] Note that changes in the region are related to the polar Ti-cation displacement and octahedron-tilt. Furthermore, one can see a red-shift in frequency for the $A_1^{(3)}$ mode of 2%Dy:NBBT in comparison to NBBT, which is consistent with Dy-doped NBT.[12] The third region above 700 cm^{-1} is related to concentration-induced longitudinal optical A_1 (LO) and E(LO) overlapping bands.[19] From the obvious variation of relatively integrated intensity and Raman shifting in the first and second region, it can be supposed that higher Dy^{3+} doping will increase chemical residual stress in the neighborhood of substitutional sites. Based on the aforementioned discussion, one can believe that the intricate variations of phonon modes are the operating mechanism for the ferroelectric phase transformation.[5,21]

Figs. 2(a)-2(f) show polarization versus *E*-field (*P*-*E*) and strain versus *E*-field (*S*-*E*) measurements at room temperature. The NBBT and 2%Dy:NBBT specimens reveal maximum values of *E*-field induced strain (denoted S_{max}) ~ 0.16% and 0.44%, respectively [see Figs. 2(a) and 2(f)]. Note that the 2%Dy:NBBT ceramic displays a 175% increase in *E*-field induced strain and a high normalized strain (S_{max}/E_{max}) of 728 pm/V [see Fig. 3(b)], which suggests an occurence of coherent domain switching at variational *E*-fields. In details, the NBBT specimen exhibits typical rectangular loop with the remnant polarization ($P_r \approx 37$ $\mu C/cm^2$) and coercive field ($E_c \approx 2.6$ kV/mm), respectively, as shown in Fig. 2(a). One sharp polarization current peak (P_1) caused by domain switching can be observed when the applied *E*-field reaches E_c. The corresponding *S*-*E* curve exhibits conventional butterfly shape, which can be ascribed to the 90° ferroelectric domain switching and domain wall expansions, as shown in Fig. 2(b). Abnormally, with *x* increasing to 1%, the *P*-*E* loop is pinched and *S*-*E* curve exhibits deformed butterfly shape with the negative strain value increasing from 0.12% (x=0) to 0.21% (x=1%). An additional polarization current peak (P_2) are shown in Figs. 2(c) and 2(e). The E_c, which is corresponding to P_1, shifts to lower *E*-field and the peak P_2 will instead. From Fig. 2(f), the *S*-*E* curve exhibits zero negative strain and the S_{max} value is close

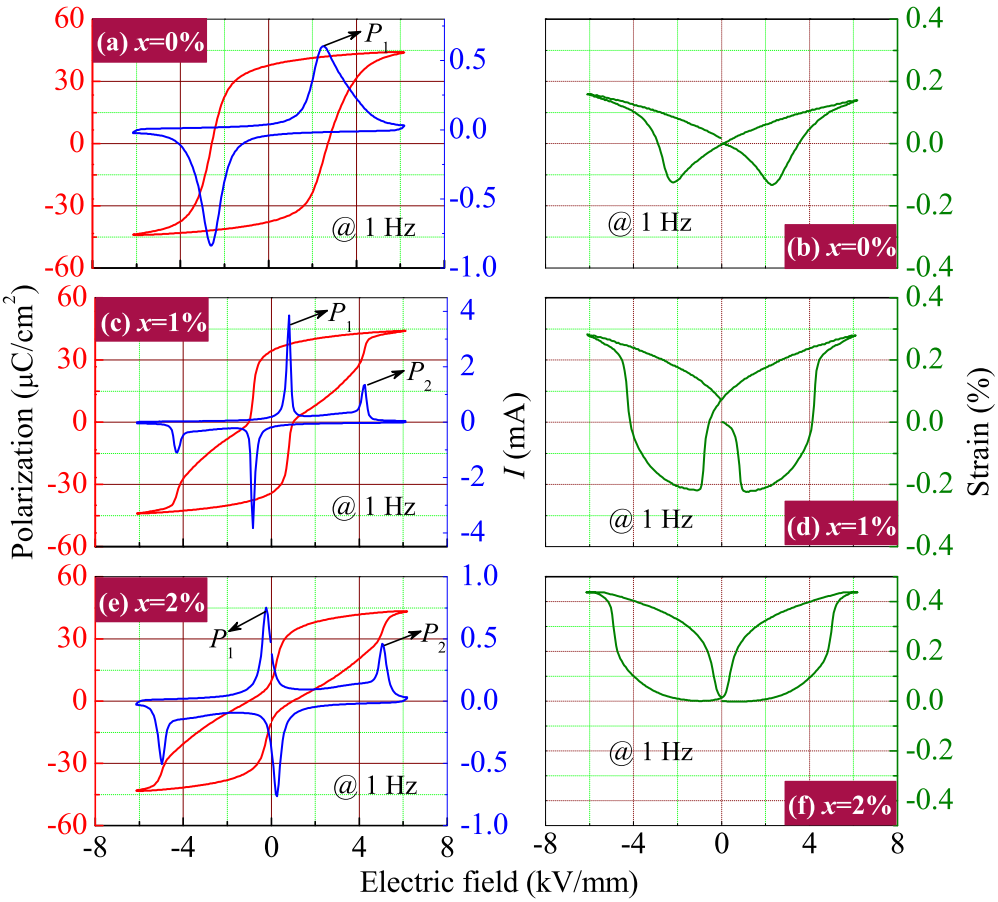

FIG. 2. (a), (c), (e) Doping level dependent ferroelectric hysteresis loops (*P*-*E*) and polarization current curves (*I*-*E*). (b), (d), (f) Bipolar strain versus electric-field (*S*-*E*) for different Dy^{3+} doping levels.

to those reported from NBT-BT single crystals.[22] Interestingly, the current peak P_1 appears along the *E*-field decreasing direction, suggesting the evolution of domain patterns from the peak P_1. Fig. 3(a) shows piezoelectric coefficient d_{33}≈201 pC/N at an optimal Dy^{3+} doping level of x=1%. The enhanced piezoelectricity can stem from the disruption of the ferroelectric long-range order structure, which leads to a nearly vanishing polarization anisotropy and thus facilitate polarization rotation between ferroelectric tetragonal and orthorhombic phases.[6,23] Wada *et al*. reported that polymorphic transition has also been shown to enhance piezoelectric properties by the instability with respective to polarization rotation.[24]

Regarding the domain switching mechanism for the xDy:NBBT ceramics with high strain response under *E*-field, we plot a schematic diagram [Figs. 3(c)-3(f)] in terms of the defect symmetry following the polar tetragonal symmetry in each domain. Fig. 3(c) explains the symmetry property of non-polar crystal and point defects (vacancies, solute atoms, antisite defects, and dopant/impurity ions) in ferroelectrics within the paraelectric cubic phase. Nevertheless, this picture is also qualitatively the similar for other ferroelectric materials because only the unified symmetry is of concern here. Now exemplified in 2%Dy:NBBT specimen, we postulate that Dy^{3+} acceptor impurity ions occupying B sites and consider that the crystal contains O^{2-} vacancies and Dy^{3+} ions. There is an equal probability of finding an O^{2-} vacancy around defect Dy^{3+}. However, in the ferroelectric phase [Fig. 3(d)], the polar tetragonal symmetry leads to the Dy^{3+} positional deviation and O^{2-} vacancies unequal probabilities. Therefore, to satisfy the minimum free energy density on the set of spontaneous state, the symmetry of short-range order distribution of defect tends to follow the crystal symmetry.[25] It is the symmetry conforming property of point defects, which is similar to martensite case.[26] However, when crystal symmetry is a polar symmetry, symmetry

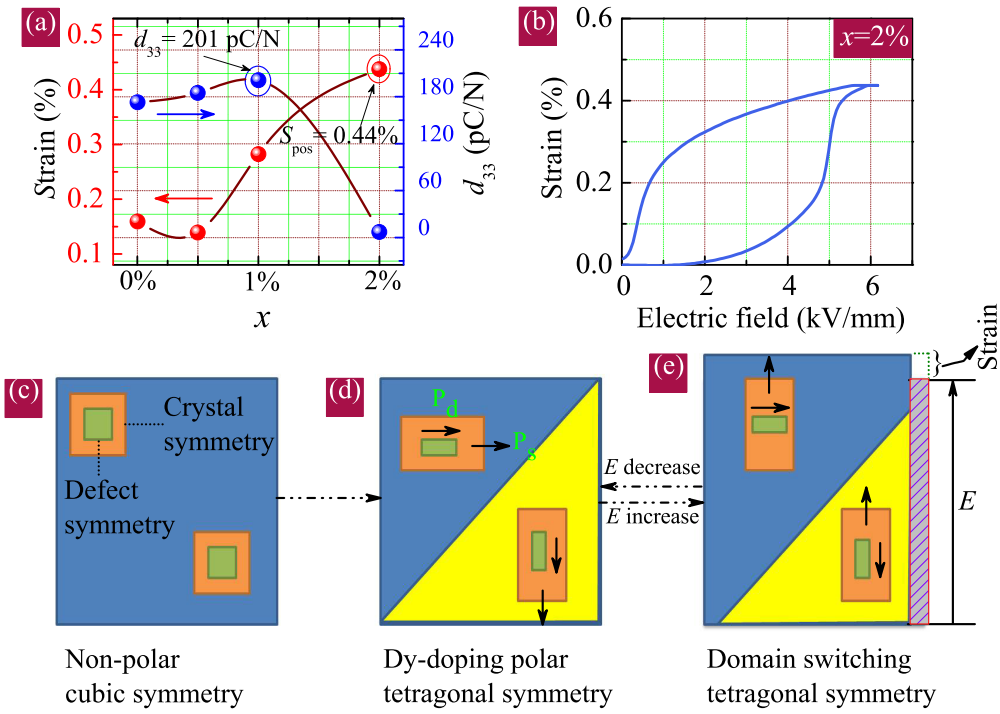

FIG. 3. (a) Doping level dependent longitudinal piezoelectric constant (d_{33}) and positive strain (S_{pos}). (b) The (P_{pos}) as a function of *E*-field for the 2%Dy:NBBT ceramic. (c) Equilibrium non-polar paraelectric cubic crystal. (d) Stable state in the polar ferroelectric state, in which defect symmetry follows crystal symmetry in every domain. (e) Unstable state after domain switching from (d) under *E*-field.

conforming property of point defects is destroyed and becomes non-centric. These non-centric distribution of the O^{2-} vacancy (which has positive effective charge) and Dy^{3+} (which has negative effective charge) forms defect dipole. Nevertheless, the cubic defect symmetry does not match the polar tetragonal crystal symmetry. For satisfying the requirement of lowest free energy for crystal, cubic defect dipole symmetry will be transformed into a polar tetragonal one. The defect dipole moment P_D will be along the polarization direction P_s, as shown in Fig. 3(d). This process contains a short-range migration of defect dipole in each domain. Then domains are located in its stable state. Since such stable domains can be switched under an elevated *E*-field, 90° domain switching occurs with P_s following the *E* direction. Correspondingly, the 90° switching of domains generates a large strain [S_{max}≈0.44%, see Figs. 3(b) and 3(e)]. Nevertheless, the strain can revert to zero when the *E*-field is back to zero because the defect symmetry and defect dipole moment cannot be rotated by oscillating *E*-field input. The unswitchable defect dipole moment provides a reverse internal field to facilitate a reverse domain switching as *E*-field decrease to zero [see Fig. 3(b)]. As the most important consequence, the giant nonlinear strain is expected in 2%Dy:NBBT ceramic, mainly due to the reversible switching of 90° domains. In fact, a theoretical simulation has been prosed based on dipolar defects induced 90° domain switching under *E*-field.[27]

Furthermore, regarding the domain structural origins for the recently reported NBT-based ceramics with large strain under *E*-field, Li *et al.* ascribed it to the multiwell structure of energy density [$W(\mathbf{s}^i, \mathbf{p}_s^i)$],[28] where $\mathbf{s}^i$ denotes spontaneous strain and $\mathbf{p}_s^i$ spontaneous polarization of the *i*th variant (i=1, …,k). Since W must be in an energy minimizing manner, the compatibility of ferroelectrics variants has become the essential condition of domain structure formation.[23] For polycrystalline materials, in a cubic to tetragonal transformation, there are three possible orientation variants with the tetragonal axes along [100], [010], or [001] directions, or six if we count those along opposite directions as separate variants.[28] On the basis of an algebra calculation, it was reported that an equiaxed tetragonal polycrystal has no 90° switching and only limited non-180° domain switching.[29] For an orthorhombic phase, there are 12 variants. According to algebra calculation,

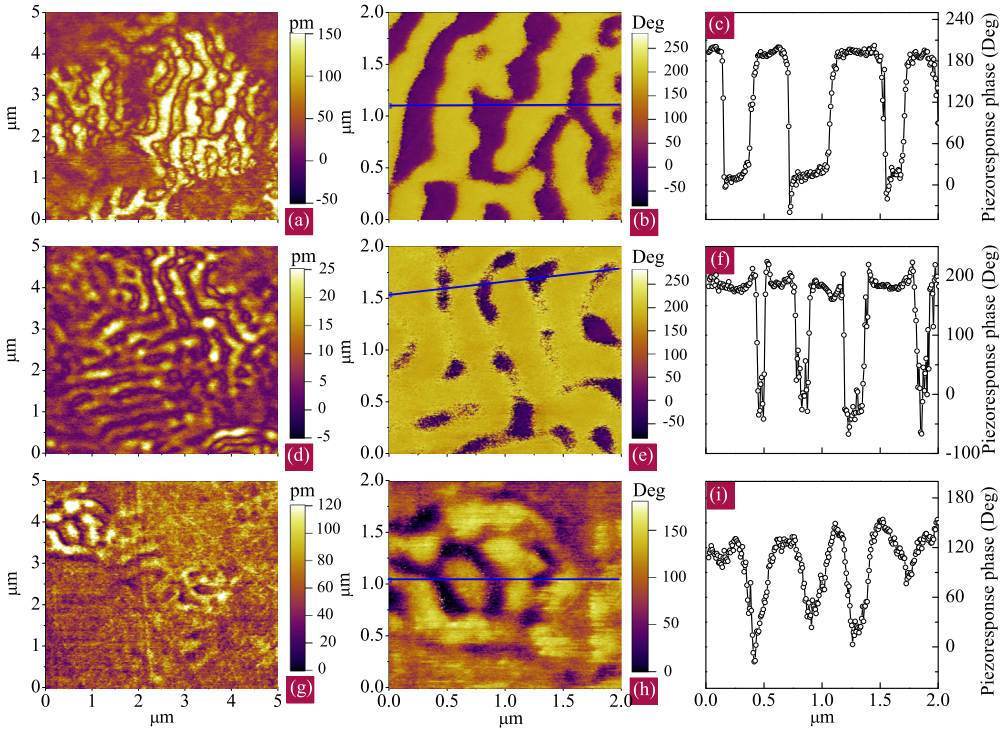

FIG. 4. (a), (d), and (g) Piezoresponse amplitude images and (b), (e), and (h) piezoresponse phase images for *x*Dy:NBBT with *x* values of 0, 1%, and 2%, respectively. Note that the scanning range is a 5 μm×5 μm. The right panel of the PFM image (c), (f), and (i) show corresponding piezoresponse phase profile generated from the line scan across the domains.

it is shown that the orthorhombic phase materials can form 60°, 90°, and 120° domain patterns. Meanwhile, for an equiaxed polycrystal with tetragonal and orthorhombic co-existence, which have 16 variants.[23] It follows that a polycrystal with co-exist phase materials would show significant amounts of 60°, 90°, 120°, and 180° domain switching with limited inter-granular constraints.

With the above knowledge that domain configuration is related to the crystal structure, the piezoresponse amplitude images [Figs. 4(a), 4(d), and 4(g)] and piezoresponse phase images [Figs. 4(b), 4(e), and 4(h)] explain why the *x*Dy:NBBT ceramics can exhibit large *E*-field induced strain. In the piezoresponse phase images, the bright contrast areas represent domains with upward polarization orientation, while dark contrast represent the opposite case. From Fig. 4(b), we can observe tweed type domain morphology (similar stripe domain) and more ordered domains in NBBT ceramic. The color contrast is more obvious and domain walls are more clear than those of 1%Dy:NBBT and 2%Dy:NBBT ceramics. From Fig. 4(e), the 1%Dy:NBBT ceramic exhibits tweed coarsen and intersected domain morphology, which indicates an increase in the number of variants and the motion of 180° domain (mostly contain reversible non-180° domain wall vibration and non-180° domain switching). Thus, one can see that the introduction of Dy^{3+} leads to a departure from local crystal symmetry to idealized cubic structure. Based on the above discussion, 1%Dy:NBBT ceramic is of tetragonal polycrystal structure. From Fig. 4(h), the contrast becomes blurred and most of the grain exhibits multidomain states with mixed dark/bright color, which can be also summarized from piezoresponse phase profile images [Figs. 4(c), 4(f), and 4(i)]. These multidomain states better prove a large strain under *E*-field due to domain switching, which suggests that 2%Dy:NBBT ceramic has a complex phase evolution caused by Dy^{3+} doping. Thus, domain switching in this polycrystalline 2%Dy:NBBT ceramic is different as the switching in one grain, which could be constrained by neighboring grain having distinct crystallographic orientation.[29,30] Therefore, 2%Dy:NBBT ceramic exhibits limited non-180° domain switching and significant amounts of 60°, 90°, and 120° switching due to limited inter-granular constraints.[29] The observed multidomain phenomenon also indicates that the domain pattern has small mismatches

on the scale of an individual domain. However, it is still compatible on a larger scale that is much smaller than the entire pattern.[31] According to the aforementioned discussion, 2%Dy:NBBT ceramic is of tetragonal and orthorhombic phase coexistence. The polycrystal material with phase co-existence will be easy to pole and result in large nonlinear macroscopic strain under *E*-field. This is a fundamental reason why the MPB region with phase co-existence has large strain induced by *E*-field. Note that the domain formation and switching described here is applicable to doping level dependent long-range ferroelectric order structure to a short-range coherence phase structure transition.

In summary, large reversible strain behavior and domain structural evolutions of lead-free piezoelectric *x*Dy:NBBT ceramics with different Dy^{3+} doping levels have been investigated. A 175% increase in the *E*-field induced strain and an intermediate phase with orthorhombic symmetry between tetragonal and rhombohedral are obtained at an optimal Dy^{3+} doping level of x=2%. Such a large strain stems from an unusual reversible 90° domain switching caused by the symmetry conforming property of point defects. The 90° reversible domain switching mechanism also reveals a new possibility to achieve large electric-field strain effect for a wide range of ferroelectric systems.

One of the authors (C. Q. Li) would like to thank Dr. Yuanyuan Zhang, Jiajun Zhu, and Fang Wang for constructive discussions. This work was financially supported by Major State Basic Research Development Program of China (Grant Nos. 2013CB922300 and 2011CB922200), Natural Science Foundation of China (Grant Nos. 11374097 and 61376129), Projects of Science and Technology Commission of Shanghai Municipality (Grant Nos. 15JC1401600, 14XD1401500, 13JC1402100 and 13JC1404200), and the Program for Professor of Special Appointment (Eastern Scholar) at Shanghai Institutions of Higher Learning.

[1] S. T. Zhang, A. B. Kounga, W. Jo, C. Jamin, K. Seifert, T. Granzow, J. Rödel, and D. Damjanovic, Adv. Mater. **21**, 4716 (2002).
[2] M. Li, H. R. Zhang, S. N. Cook, L. H. Li, J. A. Kilner, I. M. Reaney, and D. C. Sinclair, Chem. Mater. **27**, 629 (2015).
[3] Y. Guo, Y. Liu, R. L. Withers, F. Brink, and H. Chen, Chem. Mater. **23**, 219 (2011).
[4] J. Kreisel, P. Bouvier, B. Dkhil, P. A. Thomas, A. M. Glazer, T. R. Welberry, B. Chaabane, and M. Mezouar, Phys. Rev. B **68**, 014113 (2003).
[5] E. Aksel, J. S. Forrester, B. Kowalski, M. Deluca, D. Damjanovic, and J. L. Jones, Phys. Rev. B **85**, 024121 (2012).
[6] W. F. Liu and X. B. Ren, Phys. Rev. Lett. **103**, 257602 (2009).
[7] W. Jo, R. Dittmer, M. Acosta, J. Zang, C. Groh, E. Sapper, K. Wang, and J. Rödel, J. Electroceram. **29**, 71 (2012).
[8] J. Yao, N. Monsegue, M. Murayama, W. Leng, W. T. Reynolds, Q. Zhang, H. Luo, J. Li, W. Ge, and D. Viehland, Appl. Phys. Lett. **100**, 012901 (2012).
[9] E. Burcsu, G. Ravichandran, and K. Bhattacharya, Appl. Phys. Lett. **77**, 1698 (2012).
[10] C. Luo, W. Ge, Q. Zhang, J. Li, H. Luo, and D. Viehland, Appl. Phys. Lett. **101**, 141912 (2012).
[11] A. Yamaji, Y. Enomoto, K. Kinoshita, and T. Murakami, J. Am. Ceram. Soc. **60**, 97 (1977).
[12] M. Zannen, H. Khemakhem, A. Kabadou, and M. Es-Souni, J. Alloys Compds. **555**, 56 (2013).
[13] P. V. Lambeck and G. H. Jonker, Ferroelectrics **22**, 729 (1978).
[14] V. S. Postinkov, V. S. Pavlov, and S. K. Turkov, J. Phys. Chem. Solids **31**, 1785 (1970).
[15] H. J. Kleebe, S. Lauterbach, L. Silvestroni, H. Kungl, M. J. Hoffmann, E. Erdem, and R. -A. Eichel, Appl. Phys. Lett. **94**, 142901 (2009).
[16] W. Jo, J. E. Daniels, J. L. Jones, X. L. Tan, P. A. Thomas, D. Damjanovic, and J. Rödel, J. Appl. Phys. **109**, 014110 (2011).
[17] J. E. Daniels, W. Jo, J. Ro. del, and J. L. Jones, Appl. Phys. Lett. **95**, 032904 (2009).
[18] E. J. Lee, J. Jeong, and Y. H. Han, Japan. J. Appl. Phys. **43**, 8126 (2004).
[19] D. Rout, K. -S. Moon, S. -J. L. Kang, and I. W. Kim, J. Appl. Phys. **108**, 084102 (2010).
[20] S. Trujillo, J. Kreisel, Q. Jiang, J. H. Smith, P. A. Thomas, P. Bouvier, and F. Weiss, J. Phys: Condens. Matter **17**, 6587 (2005).
[21] J. Kreisel, A. M. Glazer, G. Jones, P. A. Thomas, L. Abello, and G. Lucazeau, J. Phys: Condens. Matter **12**, 3267 (2000).
[22] H. W. Zhang, H. Deng, C. Chen, L. Li, D. Lin, X. B. Li, X. Y. Zhao, H. S. Luo, and J. Yan, Scripta Mater. **75**, 50 (2014).
[23] Y. C. Shu and K. Bhattacharya, Phil. Mag. B **81**, 2021 (2001).
[24] S. Wada, K. Yako, H. Kakemoto, T. Tsurumi, and T. Kiguchi, J. Appl. Phys. **98**, 014109 (2005).
[25] X. Ren and K. Otsuka, Nature **389**, 579 (1997).
[26] Y. Murakami, S. Morito, Y. Nakajima, K. Otsuka, T. Suzuki, and T. Ohba, Mater. Lett. **21**, 275 (1994).
[27] R. Ahluwalia and W. W. Cao, Phys. Rev. B **63**, 012103 (2000).
[28] J. Y. Li and D. Liu, J. Mech. Phys. Solids **52**, 1719 (2004).
[29] J. Y. Li, R. C. Rogan, E. Üstündag, and K. Bhattacharya, Nature Mater. **4**, 776 (2005).
[30] D. Maurya, M. Murayama, A. Pramanick, W. T. Reynolds, Jr., K. An, and S. Priya, J. Appl. Phys. **113**, 114101 (2013).
[31] A. DeSimone and R. D. James, J. Mech. Phys. Solids **50**, 283 (2002).